Frontiers of Physics
https://doi.org/10.1007/s11467-020-0987-z
Front. Phys.
15(6), 63504 (2020)

RESEARCH ARTICLE

Tuning band alignment and optical properties of 2D van der Waals heterostructure via ferroelectric polarization switching

Dimuthu Wijethunge[1,2], Lei Zhang[1,2], Cheng Tang[1,2], Aijun Du[1,2,†]

[1] *School of Chemistry and Physics, Queensland University of Technology, Gardens Point Campus, Brisbane, QLD 4000, Australia*
[2] *Centre for Materials Science, Queensland University of Technology, Gardens Point Campus, Brisbane, QLD 4000, Australia*
Corresponding author. E-mail: [†] *aijun.du@qut.edu.au*
Received June 30, 2020; accepted July 28, 2020

Favourable band alignment and excellent visible light response are vital for photochemical water splitting. In this work, we have theoretically investigated how ferroelectric polarization and its reversibility in direction can be utilized to modulate the band alignment and optical absorption properties. For this objective, 2D van der Waals heterostructures (HTSs) are constructed by interfacing monolayer MoS_2 with ferroelectric In_2Se_3. We find the switch of polarization direction has dramatically changed the band alignment, thus facilitating different type of reactions. In $In_2Se_3/MoS_2/In_2Se_3$ heterostructures, one polarization direction supports hydrogen evolution reaction and another polarization direction can favour oxygen evolution reaction. These can be used to create tuneable photocatalyst materials where water reduction reactions can be selectively controlled by polarization switching. The modulation of band alignment is attributed to the shift of reaction potential caused by spontaneous polarization. Additionally, the formed type-II van der Waals HTSs also significantly improve charge separation and enhance the optical absorption in the visible and infrared regions. Our results pave a way in the design of van der Waals HTSs for water splitting using ferroelectric materials.

Keywords photocatalyst, ferroelectric, MoS_2, In_2Se_3, heterostructures, water splitting, 2D materials

1 Introduction

In the context of searching sustainable, economical, and efficient energy generation processes, nature provides perfect insight on what future energy generation should be like. In photosynthesis process, solar energy is converted into chemical energy by plants and such type of conversion can be achieved also through photocatalyst materials, even though the efficiency is far below the natural photosynthesis process. Photocatalyst material has gained immense popularity in research community since the first discovery of ZnO in 1911 [1]. Later, another popular photocatalyst, TiO_2, was reported in 1938, through production of active oxides by absorbing UV on the surface [2]. After several decades Fujishima *et al.* introduced electrochemical photolysis of water using TiO_2 and Pt electrodes [3]. Since then water splitting through solar irradiation into hydrogen and oxygen identified as the efficient reaction for solar chemical energy conversion. Later various photocatalyst such as CeO_2 [4], $BiVO_4$ [5], WO_3 [6] , CdS [7], GaN [8], WSe_2 [9], and InGaP [10] were reported. Among them $BiVO_4$ based photoanode has demonstrated the highest conversion efficiencies around 5.2% [11]. With the discovery of graphene, the use of two-dimensional (2D) materials as a photocatalyst become major focus owing to their unique characteristics such as ideal band gap, and high surface area. 2D materials such as MoS_2 [12, 13], SiP [14], g-C_3N_4 [15], InSe [16], $PdSeO_3$ [17], and In_2Se_3 [18] have shown good photocatalytic properties for water splitting.

Theoretically, a perfect efficient photocatalyst should possess a bandgap higher than 1.23 eV but not greater than 3.0 eV. Here 1.23 eV is the free energy of water splitting and band gap should be less than 3.0 eV for efficient absorbance of the solar energy [19, 20]. In addition, band edges of photocatalyst material should be aligned with potentials of hydrogen evolution reaction (HER) and oxygen evolution reaction (OER). Conduction Band Minimum (CBM) should be higher than -4.44 eV (pH = 0 for efficient HER reaction) [21]. Valence Band Minimum (VBM) should be lower than -5.67 eV (pH = 0), which is the potential for OER reaction [21]. Eqs. (1) and (2) illustrate the OER and HER where electrons and holes are denoted by e and h, respectively. Additionally, e and h must be well separated. In general, it is extremely chal-

*Special Topic: Heterojunction and Its Applications (Ed. Chenghua Sun).
arXiv: 2009.00961.

© Higher Education Press 2020

lenging to find an efficient photocatalytic material which satisfies all these requirements

$$H_2O + 2h^+ \longrightarrow 2H^+ + \frac{1}{2}O_2, \quad (1)$$

$$2H^+ + 2e^- \longrightarrow H_2. \quad (2)$$

Ferroelectric material exhibits spontaneous polarization in the absence of external electric field. Some research works have demonstrated influence of changing polarization direction on catalytic surface absorption and desorption [22], Schottky tunnel barrier [23] , e–h charge separation [24], and bandstructure engineering [25]. Recently few 2D ferroelectric materials with out-of-plane polarization have been discovered and synthesized [26–28]. One interesting question is to investigate possibility of improving the photocatalysis performance by forming van der Waals Heterostructures (HTSs) with ferroelectric materials. It is highly expected that ferroelectric materials with spontaneous polarization and reversibility of the polarization direction can significantly modulate the band alignment. Additionally, by forming Type-II van der Waals HTSs with ferroelectric materials, it can also facilitate charge separation and enhance optical absorption in photocatalyst [29]. 2D α-In_2Se_3 with a band gap of 1.3 eV is an experimentally realized ferroelectric material that have demonstrated potential for water splitting applications [18, 30]. 2D In_2Se_3 possesses considerable out-of-plane ferroelectric polarization and the band gap can be reduced when it forms a vertical HTS with WSe_2 monolayers [31]. In_2Se_3/MoS_2 HTS has been experimentally synthesized and used as a photoanode in water splitting [32]. Optical absorption properties of In_2Se_3/MoS_2 HTS has been improved compared to intrinsic In_2Se_3 and MoS_2 [33].

2D MoS_2 has a bandgap around 1.8 eV [34] which is larger than 1.23 eV and its band alignment support both HER and OER [12]. MoS_2 has good carrier mobility and high surface to volume ratio butcharge recombination is much higher considering the amount of charge generated. It also has the leverage to reduce from its original band gap of 1.8 eV to 1.23 eV, which automatically increases the light absorption at infrared wavelength. Studies have shown, constructing HTS with certain materials can reduce both band gap and charge recombination in MoS_2 [35–37] . In HTSs, charge recombination is reduced greatly when CBM and VBM appears in two different layers.

In this work, we have constructed HTSs using 2D MoS_2 and ferroelectric In_2Se_3 and found that band position can only support HER or OER depending on the ferroelectric polarization direction. When MoS_2 layer is sandwiched between top and bottom In_2Se_3 to form $In_2Se_3/MoS_2/In_2Se_3$ HTS, three distinct polarization states can be produced and each exhibit different band alignment with water reduction potential. One polarization state facilitates both HER and OER and the other polarizations states only facilitate either OER or HER. This allows us to shift the water reduction potentials in photocatalyst material simply by switching ferroelectric polarization in ferroelectric materials, potentially enhance the photocatalysis efficiency in water splitting. Additionally, the formed type-II van der Waals HTSs also significantly improve charge separation and enhance the optical absorption in the visible and infrared regions.

2 Methodology

All calculations were conducted by using density functional theory (DFT) with the assistance of Vienna Ab Initio Simulation Package (VASP) [38]. Core and valence electrons were interpreted using projected-wave (PAW) argument method [39, 40]. Both Perdew, Burke, and Ernzerh (PBE) method [41] and Heyd–Scuseria–Ernzerhof (HSE) method [42] were used in the calculation of bandstructure. DFT-D3 methods was used to incorporate long range van der Waals interactions in HTSs [43]. Vacuum region of 20 Å was maintained to prevent interaction between periodic images. Cut-off energy of 500 eV was used and the convergence criteria of forces on the atoms were set to -0.001 eV/Å and energy convergence criteria was set to 1E$-$06. 5×5×1 and 7×7×1 gamma centred k-point meshes were used for the geometry relaxations and electron structure calculations, respectively.

2D In_2Se_3 and MoS_2 crystal structures were illustrated in Figs. 1(a)–(d). Table 1 shows the calculated lattice parameters for In_2Se_3 and MoS_2 and those are in

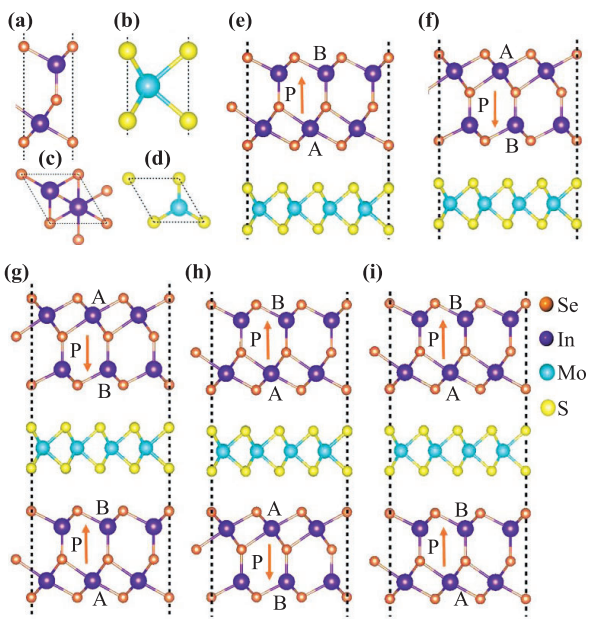


Fig. 1 Side view of **(a)** In_2Se_3 **(b)** MoS_2 and top view of **(c)** In_2Se_3 **(d)** MoS_2 monolayers. Side view of **(e)** type-A **(f)** type-B, In_2Se_3/MoS_2 heterostructures and **(g)** type-BB **(h)** type-AA **(i)** type-AB, $In_2Se_3/MoS_2/In_2Se_3$, heterostructures. Polarization direction is indicated by the arrow.

Table 1 Lattice parameters of Monolayer In_2Se_3 and MoS_2 unit cells, compared with reference values.

	a, b (Å) this work	c (Å) this work	Ref a, b (Å)	Ref c (Å)
In_2Se_3	4.07	6.84	4.10 [31], 4.11 [18]	6.8 [31]
MoS_2	3.16	3.13	3.22 [44], 3.18 [12]	3.17 [45]

good agreement with the experimental values. First, 2D In_2Se_3/MoS_2 HTSs were constructed using 3×3 In_2Se_3 and 4×4 MoS_2 unit cells to achieve minimum lattice mismatch (3%). Two different polarization states (type-A and type-B) for 2D In_2Se_3/MoS_2 HTSs were illustrated in Figs. 1(e) and (f). Next, $In_2Se_3/MoS_2/In_2Se_3$ HTSs were constructed as shown in Figs. 1(g)–(i) by sandwiching MoS_2 between In_2Se_3 layers. Based on polarization direction, three different polarizations states can be found and they were denoted as type-BB, type-AA, and type-AB. Reversing of the polarization occurs through rearrangement of the contacted surfaces (A and B). Naming of the HTSs are based on which side of In_2Se_3 is in contact with MoS_2. For example, HTS is named as type-AA, when the side A of In_2Se_3 layers are in contact with MoS_2 from both top and bottom sides.

3 Results and discussion

3.1 Methodology

Bandstructure of the intrinsic In_2Se_3 and MoS_2 was calculated using both HSE and PBE methods. As given in Table 2, our calculated values have good agreement to both experimental and previous theoretical calculations. According to the results, MoS_2 bandgap was accurate when calculated by PBE method, while bandgap of In_2Se_3 was accurate when calculated using HSE method.

Binding energies (E_b) of all HTSs were calculated using Eq. (3) to check the stability of HTSs. Here E_{tot}, $E_{In_2Se_3}$, and E_{MoS_2} are the total energy of the system, energy of In_2Se_3 layer and energy of MoS_2 layer, respectively. For the HTSs with single layer of In_2Se_3, one $E_{In_2Se_3}$ term can be neglected. Binding energies of all HTSs having

Table 2 Bandgap of monolayer In_2Se_3 and MoS_2 calculated using PBE and HSE methods and values obtained from reference calculations done by PBE, HSE, and experimental methods.

	PBE, this work	HSE, this work	PBE	HSE	Experiment
QL In_2Se_3	0.82 eV	1.51 eV	0.78 eV [31], 0.77 eV [46]	1.46 eV [31]	1.3 eV [30]
Monolayer MoS_2	1.75 eV	2.07 eV	1.9 eV [47], 1.78 eV [48], 1.70 eV [49]	2.01 eV [50]	1.8 eV [34]

Table 3 Calculated binding energies of all heterostructures.

	E_{tot}(eV)	$E_{In_2Se_3}$(eV)	E_{MoS_2}(eV)	E_b(eV)
In_2Se_3/MoS_2 type-A	−529.584	−170.907	−356.628	−2.049
In_2Se_3/MoS_2 type-B	−529.428	−170.907	−356.628	−1.893
$In_2Se_3/MoS_2/In_2Se_3$ type-AB	−702.985	−170.907	−356.628	−4.543
$In_2Se_3/MoS_2/In_2Se_3$ type-AA	−702.955	−170.907	−356.628	−4.513
$In_2Se_3/MoS_2/In_2Se_3$ type-BB	−702.732	−170.907	−356.628	−4.290

negative values as indicated in Table 3, suggesting, HTSs are stable and energy wise favourable to form

$$E_b = E_{tot} - E_{In_2Se_3(top)} - E_{MoS_2} - E_{In_2Se_3(bottom)}. \quad (3)$$

3.2 In_2Se_3/MoS_2 heterostructures

Bandstructure and contribution of each layer to its bands have been investigated in In_2Se_3/MoS_2 HTS as illustrated in Fig. 2. Type-A HTS shows band gap of 0.66 eV (PBE method) which is a reduced bandgap compared to intrinsic In_2Se_3 and MoS_2. On the other hand, type-B HTS has band gap of 0.84 eV (PBE method) which is similar to the band gap of In_2Se_3. According to the bandstructure of type-A HTS, valence band is contributed by MoS_2 layer and conduction band is contributed by In_2Se_3 layer. Hence charge recombination is greatly reduced owing to transferring of holes and electrons into two different layers. But in type-B configuration, both conduction and valence bands are mainly contributed by the In_2Se_3 layer, thus charge separation is not effectively facilitated. According to research, intrinsic In_2Se_3 also has better charge separation compared to MoS_2 monolayer due to its inbuilt polarization [18].

Figures 3(a) and (b) illustrate the electrostatic potential

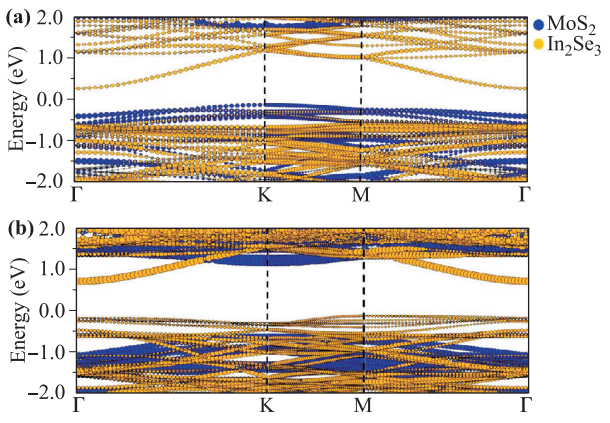


Fig. 2 Electronic bandstructure of **(a)** type A **(b)** type B In_2Se_3/MoS_2 heterostructure, calculated using PBE method. Contribution to each band from MoS_2 and In_2Se_3 layers are indicated in different colours.

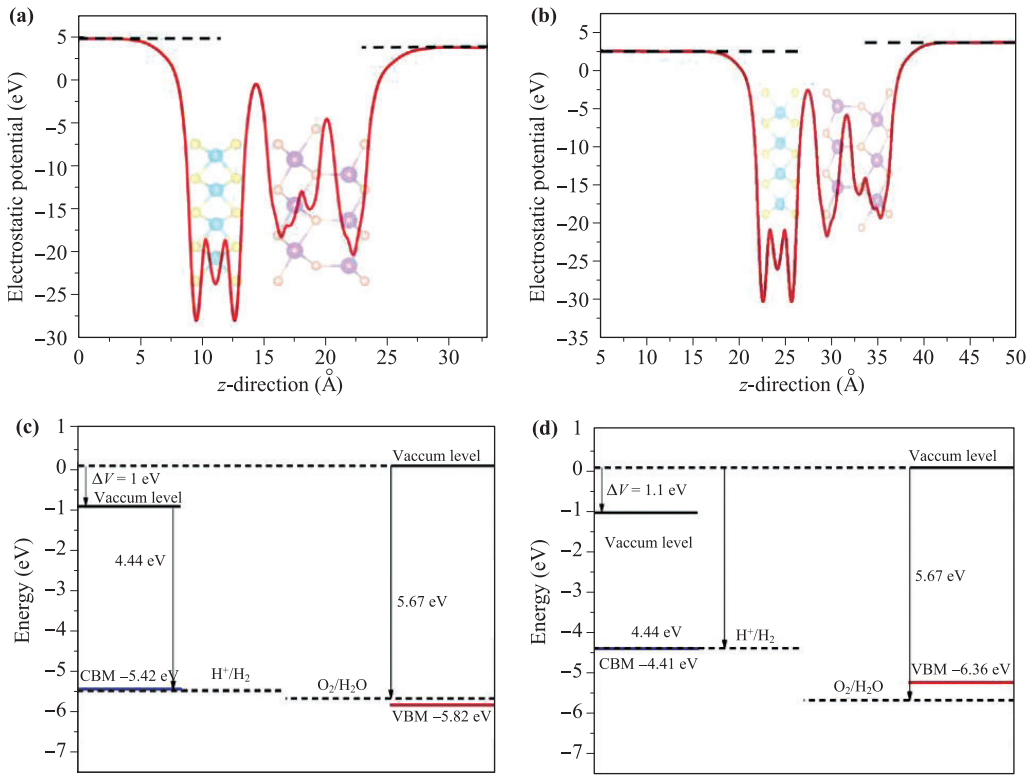


Fig. 3 Electrostatic potential of **(a)** type-A **(b)** type-B HTSs and alignment of VBM and CBM respect to HER and OER potentials of **(c)** type-A **(d)** type-B HTSs, calculated based on PBE method.

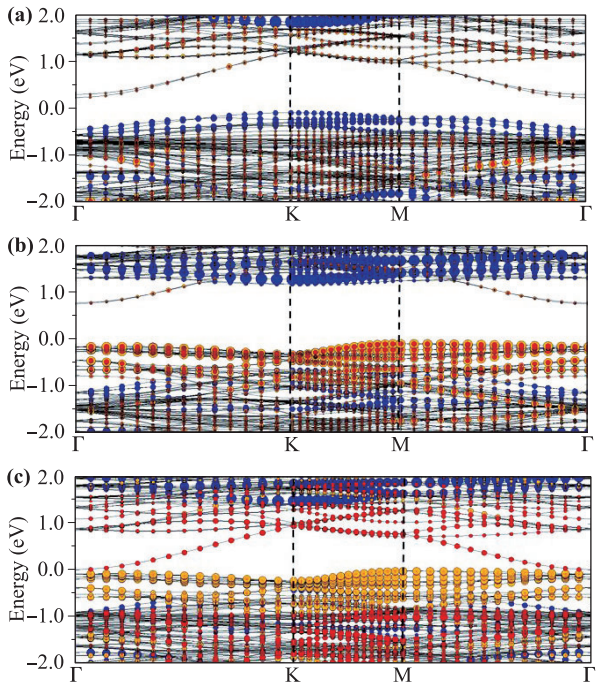


Fig. 4 Electronic bandstructure of **(a)** type-AA **(b)** type-BB **(c)** type-AB $In_2Se_3/MoS_2/In_2Se_3$ heterostructure, calculated using PBE method. Contributions to each band from MoS_2, In_2Se_3 bottom layer and In_2Se_3 top layer indicated in different colours.

(eV) of both HTSs and it shows different vacuum levels at each end owing to the inbuilt polarization. Figures 3(c) and (d) show the band alignment of type-A and type-B configurations. Type-A have CBM above the HER potential and VBM below the OER potential, thus, it supports both reactions. However, in type-B configuration, VBM is higher than the OER potential and CBM is below the HER potential. Therefore, only HER is supported in type-B configuration. Results exhibit change of polarization direction has strong impact on band alignment. Through close observation, it can be seen that spontaneous polarization also plays critical role in the context of band aligning. In type-A HTS, CBM is −5.42 eV and yet it is above the HER potential. This happens as a result of different vacuum levels at both ends. Only In_2Se_3 have contributed to the CBM and vacuum level is lower at the end of In_2Se_3. Therefore, when considering HER potential respect to the vacuum level at the side of In_2Se_3, it becomes lower than the CBM. On the other hand, in type-B HTS, both CBM and VBM occurs in In_2Se_3 layer,which has the greater vacuum level. Therefore, the both potential values taken respect to same vacuum level. This feature is unique to polarized materials and it can assist better band alignment in photocatalyst materials.

3.3 $In_2Se_3/MoS_2/In_2Se_3$ heterostructures

Here, HTSs were constructed by sandwiching the MoS_2 layer between In_2Se_3 layers. In this arrangement, polar-

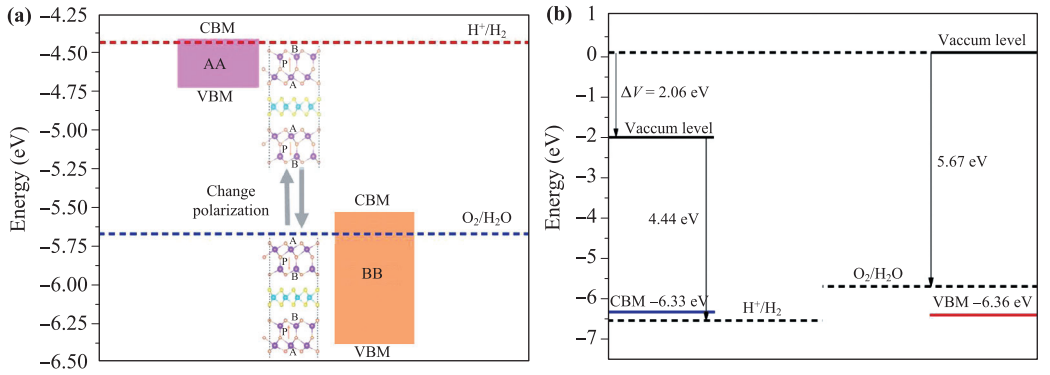


Fig. 5 Alignment of VBM and CBM respect to HER and OER potentials of **(a)** type AA, type BB, and **(b)** type AB HTSs, which are calculated using PBE method.

ization becomes stronger and its controllability can be improved. Based on polarization direction, three states, namely, AA, BB, and AB can be identified. In type-AA and type-BB HTSs, In_2Se_3 layers have polarization directions opposing to each other, hence HTSs have zero net spontaneous polarization. In AB HTS, polarization direction of the two layers are in same direction, thus, it is subjected to very high spontaneous polarization. Figure 4 shows the band structure and contribution to bands from each layer. In type-AA, CBM is contributed by both top and bottom In_2Se_3 layers and VBM is by the MoS_2. In type-BB, both CBM and VBM occur in both In_2Se_3 layers. In type-AB CBM occurs in top In_2Se_3 layer and VBM occurs in bottom In_2Se_3 layer. Therefore, type-AA and type-AB types have good charge separation while charge separation has not improved in type-BB.

As illustrated in Fig. 5, type-AA configuration supports only HER and type-BB configuration supports only OER. But Type-AB configuration supports both reactions owing to assistance from existing inbuilt spontaneous polarization. This dramatic change of band alignment respect to the direction of polarization can lead to tuneable photocatalyst materials which its selectivity and efficiency of the chemical reactions can be controlled by changing the polarization direction.

Finally, optical absorption coefficient of all HTSs, MoS_2 and In_2Se_3 have been studied as shown in Fig. 6. All HTSs except type-B HTS have shown increased optical absorption coefficient compared to In_2Se_3 and MoS_2 around the ultraviolet (UV) region. In visual light region, all HTSs, MoS_2, and In_2Se_3 have shown similar absorption coefficient values. As highlighted in Fig. 6(b), optical absorption at infrared region also has shown considerable increase in all HTSs compared to MoS_2. The increase of infrared light absorption occurs due to reduction of bandgap in HTSs.

4 Conclusion

In this work, In_2Se_3/MoS_2 heterostructures with two polarization states, namely, type-A and type-B and $In_2Se_3/MoS_2/In_2Se_3$ heterostructures with three polarization states, namely, type-AA, type-BB, and type-AB have

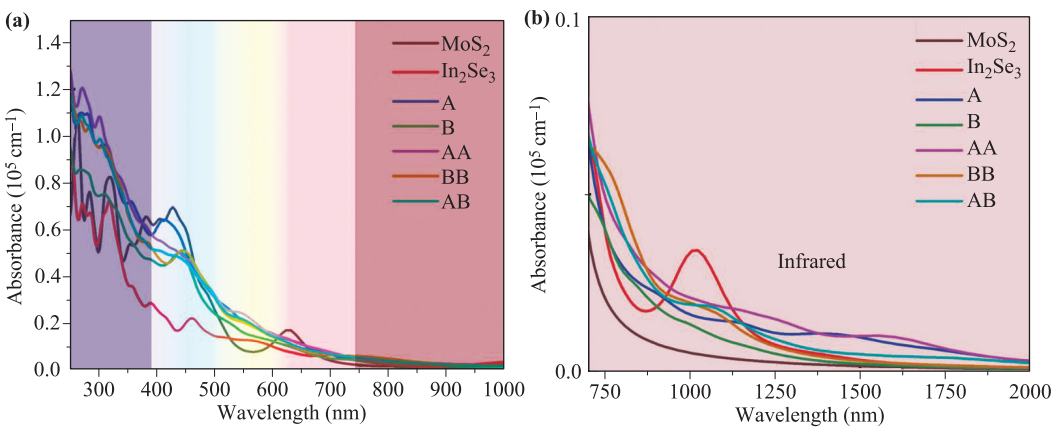


Fig. 6 Optical absorption spectra in (MoS_2 monolayer, In_2Se_3 monolayer, type-A, type-B, type-AA, type-BB, and type-AB heterostructures represented by black, red, blue, green, violet, orange, and cyan lines, respectively) **(a)** UV, visible light and infrared wavelengths, **(b)** Extended infrared wavelengths, calculated based on PBE calculations.

been studied. Type-A and Type-AB HTSs support both OER and HER. Type-B and type-AA HTSs only support HER while Type-BB HTS only supports OER. Through HTSs formation, charge separation can be enhanced in photocatalyst materials as reflected by type-A, type-AA, and type-AB configurations. All HTSs have shown increased optical absorption coefficient at UV and infrared region of the solar spectrum compared to monolayer MoS_2 and In_2Se_3.

The ability to change band alignment through altering the polarization direction is one of the important findings of this work. This feature is evident in type-AA, type-BB, and type-AB HTSs which their band alignments were drastically changed respective to the polarization direction. Applying this principle, external electric field can be used to reverse the polarization and change the material properties from photoanode to photocathode or vice versa. This also allows to change reaction paths according to the concentration of the products generated in the solution. If the products of one reaction is greater than the other, then the polarization direction can be changed to facilitate the other reaction using the same photocatalyst material. Interestingly, fast switching between $In_2Se_3/MoS_2/In_2Se_3$ three polarization states (AA, AB, BB) perhaps can provide an interesting result in water splitting applications. Another important finding is how the spontaneous polarization have shifted OER or HER potential values as shown in type-A and type-AB HTS configurations to facilitate the band alignment. Overall results of this work provide valuable insight on how ferroelectric materials can be used in photocatalyst application to improve their performance and may lead to development of next generation tuneable photocatalyst for water splitting.

Acknowledgements We highly acknowledge Queensland University of Technology (QUT) and National Computational Infrastructure (NCI) Australia for providing high performance computing (HPC) facilities to undertake this project.

References

1. J. M. Coronado, A Historical Introduction to Photocatalysis, in: Design of Advanced Photocatalytic Materials for Energy and Environmental Applications, J. M. Coronado, F. Fresno, M. D. Hernández-Alonso, and R. Portela (Eds.), Springer London: London, 2013, pp 1–4
2. C. F. Goodeve and J. A. Kitchener, The mechanism of photosensitisation by solids, *Trans. Faraday Soc.* 34(0), 902 (1938)
3. A. Fujishima and K. Honda, Electrochemical photolysis of water at a semiconductor electrode, *Nature* 238(5358), 37 (1972)
4. D. Channei, B. Inceesungvorn, N. Wetchakun, S. Ukritnukun, A. Nattestad, J. Chen, and S. Phanichphant, Photocatalytic degradation of methyl orange by CeO_2 and Fe-doped CeO_2 films under visible light irradiation, *Sci. Rep.* 4(1), 5757 (2014)
5. F. F. Abdi, L. Han, A. H. M. Smets, M. Zeman, B. Dam, and R. van de Krol, Efficient solar water splitting by enhanced charge separation in a bismuth vanadate-silicon tandem photoelectrode, *Nat. Commun.* 4(1), 2195 (2013)
6. P. Dong, G. Hou, X. Xi, R. Shao, and F. Dong, WO_3-based photocatalysts: Morphology control, activity enhancement and multifunctional applications, *Environ. Sci. Nano* 4(3), 539 (2017)
7. M. Luo, Y. Liu, J. Hu, H. Liu, and J. Li, One-pot synthesis of CdS and Ni-doped CdS hollow spheres with enhanced photocatalytic activity and durability, *ACS Appl. Mater. Interfaces* 4(3), 1813 (2012)
8. T. Kida, Y. Minami, G. Guan, M. Nagano, M. Akiyama, and A. Yoshida, Photocatalytic activity of gallium nitride for producing hydrogen from water under light irradiation, *J. Mater. Sci.* 41(11), 3527 (2006)
9. A. Eftekhari, Tungsten dichalcogenides (WS_2, WSe_2, and WTe_2): Materials chemistry and applications, *J. Mater. Chem. A* 5(35), 18299 (2017)
10. P. Varadhan, H. C. Fu, Y. C. Kao, R. H. Horng, and J. H. He, An efficient and stable photoelectrochemical system with 9% solar-to-hydrogen conversion efficiency via InGaP/GaAs double junction, *Nat. Commun.* 10(1), 5282 (2019)
11. L. Han, F. F. Abdi, R. van de Krol, R. Liu, Z. Huang, H. J. Lewerenz, B. Dam, M. Zeman, and A. H. M. Smets, Efficient water-splitting device based on a bismuth vanadate photoanode and thin-film silicon solar cells, *ChemSusChem* 7(10), 2832 (2014)
12. Y. Li, Y. L. Li, C. M. Araujo, W. Luo, and R. Ahuja, Single-layer MoS_2 as an efficient photocatalyst, *Catal. Sci. Technol.* 3(9), 2214 (2013)
13. J. Mao, Y. Wang, Z. Zheng, and D. Deng, The rise of two-dimensional MoS_2 for catalysis, *Front. Phys.* 13(4), 138118 (2018)
14. Z. Ma, J. Zhuang, X. Zhang, and Z. Zhou, SiP monolayers: New 2D structures of group IV-V compounds for visible-light photohydrolytic catalysts, *Front. Phys.* 13(3), 138104 (2018)
15. Y. Wang, M. Miao, J. Lv, L. Zhu, K. Yin, H. Liu, and Y. Ma, An effective structure prediction method for layered materials based on 2D particle swarm optimization algorithm, *J. Chem. Phys.* 137(22), 224108 (2012)
16. H. L. Zhuang and R. G. Hennig, Single-layer group-III monochalcogenide photocatalysts for water splitting, *Chem. Mater.* 25(15), 3232 (2013)
17. M. Qiao, J. Liu, Y. Wang, Y. Li, and Z. Chen, $PdSeO_3$ monolayer: Promising inorganic 2D photocatalyst for direct overall water splitting without using sacrificial reagents and cocatalysts, *J. Am. Chem. Soc.* 140(38), 12256 (2018)
18. P. Zhao, Y. Ma, X. Lv, M. Li, B. Huang, and Y. Dai, Two-dimensional III_2-VI_3 materials: Promising photocatalysts for overall water splitting under infrared light spectrum, *Nano Energy* 51, 533 (2018)
19. R. M. Navarro Yerga, M. C. Álvarez Galván, F. del Valle, J. A. Villoria de la Mano, and J. L. G. Fierro, Water splitting on semiconductor catalysts under visible-light irradiation, *ChemSusChem* 2(6), 471 (2009)

20. A. Kudo and Y. Miseki, Heterogeneous photocatalyst materials for water splitting, *Chem. Soc. Rev.* 38(1), 253 (2009)
21. M. Ni, M. K. H. Leung, D. Y. C. Leung, and K. Sumathy, A review and recent developments in photocatalytic water-splitting using TiO_2 for hydrogen production, *Renew. Sustain. Energy Rev.* 11(3), 401 (2007)
22. A. Kakekhani and S. Ismail-Beigi, Ferroelectric-based catalysis: Switchable surface chemistry, *ACS Catal.* 5(8), 4537 (2015)
23. X. Liu, Y. Wang, J. D. Burton, and E. Y. Tsymbal, Polarization-controlled Ohmic to Schottky transition at a metal/ferroelectric interface, *Phys. Rev. B* 88(16), 165139 (2013)
24. D. Kim, H. Han, J. H. Lee, J. W. Choi, J. C. Grossman, H. M. Jang, and D. Kim, Electron hole separation in ferroelectric oxides for efficient photovoltaic responses, *Proc. Natl. Acad. Sci. USA* 115(26), 6566 (2018)
25. D. Wijethunge, C. Tang, C. Zhang, L. Zhang, X. Mao, and A. Du, Bandstructure engineering in 2D materials using ferroelectric materials, *Appl. Surf. Sci.* 513, 145817 (2020)
26. F. Liu, L. You, K. L. Seyler, X. Li, P. Yu, J. Lin, X. Wang, J. Zhou, H. Wang, H. He, S. T. Pantelides, W. Zhou, P. Sharma, X. Xu, P. M. Ajayan, J. Wang, and Z. Liu, Room-temperature ferroelectricity in $CuInP_2S_6$ ultrathin flakes, *Nat. Commun.* 7(1), 12357 (2016)
27. S. Yuan, X. Luo, H. L. Chan, C. Xiao, Y. Dai, M. Xie, and J. Hao, Room-temperature ferroelectricity in $MoTe_2$ down to the atomic monolayer limit, *Nat. Commun.* 10(1), 1775 (2019)
28. A. Chandrasekaran, A. Mishra, and A. K. Singh, Ferroelectricity, antiferroelectricity, and ultrathin 2D electron/hole gas in multifunctional monolayer MXene, *Nano Lett.* 17(5), 3290 (2017)
29. J. Low, J. Yu, M. Jaroniec, S. Wageh, and A. A. Al-Ghamdi, *Heterojunction Photocatalysts* 29(20), 1601694 (2017)
30. C. Cui, W. J. Hu, X. Yan, C. Addiego, W. Gao, Y. Wang, Z. Wang, L. Li, Y. Cheng, P. Li, X. Zhang, H. N. Alshareef, T. Wu, W. Zhu, X. Pan, and L. J. Li, Intercorrelated in-plane and out-of-plane ferroelectricity in ultrathin two-dimensional layered semiconductor In_2Se_3, *Nano Lett.* 18(2), 1253 (2018)
31. W. Ding, J. Zhu, Z. Wang, Y. Gao, D. Xiao, Y. Gu, Z. Zhang, and W. Zhu, Prediction of intrinsic two-dimensional ferroelectrics in In_2Se_3 and other III_2-VI_3 van der Waals materials, *Nat. Commun.* 8(1), 14956 (2017)
32. Y. Jiang, Q. Wang, L. Han, X. Zhang, L. Jiang, Z. Wu, Y. Lai, D. Wang, and F. Liu, Construction of In_2Se_3/MoS_2 heterojunction as photoanode toward efficient photoelectrochemical water splitting, *Chem. Eng. J.* 358, 752 (2019)
33. J. R. Zhang, X. Z. Deng, B. Gao, L. Chen, C. T. Au, K. Li, S. F. Yin, and M. Q. Cai, Theoretical study on the intrinsic properties of In_2Se_3/MoS_2 as a photocatalyst driven by near-infrared, visible and ultraviolet light, *Catal. Sci. Technol.* 9(17), 4659 (2019)
34. K. F. Mak, C. Lee, J. Hone, J. Shan, and T. F. Heinz, Atomically thin MoS_2: A new direct-gap semiconductor, *Phys. Rev. Lett.* 105(13), 136805 (2010)
35. H. Li, K. Yu, Z. Tang, H. Fu, and Z. Zhu, High photocatalytic performance of a type-II α-MoO_3@MoS_2 heterojunction: From theory to experiment, *Phys. Chem. Chem. Phys.* 18(20), 14074 (2016)
36. Q. Li, N. Zhang, Y. Yang, G. Wang, and D. H. L. Ng, High efficiency photocatalysis for pollutant degradation with MoS_2/C_3N_4 heterostructures, *Langmuir* 30(29), 8965 (2014)
37. F. Li, C. Shi, D. Wang, G. Cui, P. Zhang, L. Lv, and L. Chen, Improved visible-light absorbance of monolayer MoS_2 on AlN substrate and its angle-dependent electronic structures, *Phys. Chem. Chem. Phys.* 20(46), 29131 (2018)
38. G. Kresse and J. Furthmüller, Efficient iterative schemes for ab initio total-energy calculations using a plane-wave basis set, *Phys. Rev. B* 54(16), 11169 (1996)
39. G. Kresse and D. Joubert, From ultrasoft pseudopotentials to the projector augmented-wave method, *Phys. Rev. B* 59(3), 1758 (1999)
40. P. E. Blöchl, Projector augmented-wave method, *Phys. Rev. B* 50(24), 17953 (1994)
41. J. P. Perdew, K. Burke, and M. Ernzerhof, Generalized gradient approximation made simple, *Phys. Rev. Lett.* 77(18), 3865 (1996)
42. J. Heyd, G. E. Scuseria, and M. Ernzerhof, Hybrid functionals based on a screened Coulomb potential, *J. Chem. Phys.* 118(18), 8207 (2003)
43. S. Grimme, J. Antony, S. Ehrlich, and, H. Krieg, A consistent and accurate *ab initio* parametrization of density functional dispersion correction (DFT-D) for the 94 elements H-Pu, *J. Chem. Phys.* 132(15), 154104 (2010)
44. C. Ataca, M. Topsakal, E. Aktürk, and S. Ciraci, A comparative study of lattice dynamics of three- and two-dimensional MoS_2, *J. Phys. Chem. C* 115(33), 16354 (2011)
45. P. Joensen, R. F. Frindt, and S. R. Morrison, Single-layer MoS_2, *Mater. Res. Bull.* 21(4), 457 (1986)
46. Z. Xie, F. Yang, X. Xu, R. Lin, and L. M. Chen, Functionalization of α-In_2Se_3 monolayer via adsorption of small molecule for gas sensing, *Front. Chem.* 6, 430 (2018)
47. A. Kuc, N. Zibouche, and T. Heine, Influence of quantum confinement on the electronic structure of the transition metal sulfide TS_2, *Phys. Rev. B* 83(24), 245213 (2011)
48. S. Lebègue and O. Eriksson, Electronic structure of two-dimensional crystals from *ab initio* theory, *Phys. Rev. B* 79(11), 115409 (2009)
49. C. Ataca and S. Ciraci, Functionalization of single-layer MoS_2 honeycomb structures, *J. Phys. Chem. C* 115(27), 13303 (2011)
50. K. Kośmider and J. Fernández-Rossier, Electronic properties of the MoS_2–WS_2 heterojunction, *Phys. Rev. B* 87(7), 075451 (2013)